Supplement of Geosci. Model Dev., 14, 5891–5913, 2021
https://doi.org/10.5194/gmd-14-5891-2021-supplement

Geoscientific Model Development
Open Access

Supplement of

Using the International Tree-Ring Data Bank (ITRDB) records as century-long benchmarks for global land-surface models

Jina Jeong et al.

Correspondence to: Jina Jeong (j.jeong@vu.nl)

1. The land-surface model ORCHIDEE

ORCHIDEE (Ducoudré, Laval, & Perrier, 1993; Krinner et al., 2005) is the land-surface model of the IPSL (Institute Pierre Simon Laplace) Earth system model. Hence, by design, it can be coupled to an atmospheric global circulation model. In a coupled setup, the atmospheric conditions affect the land-surface and the land-surface, in turn, affects the atmospheric conditions. However, when a study focuses on changes in the land-surface rather than on the interactions with climate, it can also be run as a stand-alone land-surface model. In both configurations the model receives atmospheric conditions such as precipitation, temperature, humidity, and incoming solar radiation, CO_2 to mention the major ones, the so-called climate forcing. Both configurations can cover any area ranging from the global domain to regional domains and down to a single grid point for the stand-alone case.

Although ORCHIDEE does not enforce a spatial or temporal resolution, the model does use a spatial grid and equidistant time steps. The spatial resolution is an implicit user setting that is determined by the coarsest resolution of its drivers, i.e., the climate forcing and the boundary conditions, namely the vegetation distribution and the soil map. Although the temporal resolution is not fixed, the processed were formalized at given time step: half-hourly (i.e. photosynthesis and energy budget), daily (i.e. net primary production), and annual (i.e. vegetation dynamics). Hence, meaningful simulations have a temporal resolution between 1 minute and 1 hour for the energy balance, water balance, and photosynthesis calculations.

ORCHIDEE builds on the concept of meta-classes to describe vegetation distribution. By default, it distinguishes 13 meta-classes (one for bare soil, eight for forests, two for grasslands, and two for croplands). Each meta-class can be subdivided into an unlimited number of plant

functional types (PFTs). When simulations make use of species-specific parameters and age classes, several PFTs belonging to a single meta-class will be defined. Biogeochemical and biophysical variables are calculated for each PFT or groups of PFTs (i.e. soil hydrology is computed for all tree PFTs together).

ORCHIDEE is not an individual based model but it represents forest stand complexity and stand dynamic with diameter and age classes. Each class contains a number of individuals that represent the mean state of the class. Therefore, each diameter class contains a single modelled tree that is replicated multiple times. At the start of a simulation, each PFT contains a user-defined number of stem diameter classes. This number is held constant, whereas the boundaries of the classes are adjusted throughout a simulation to accommodate for temporal evolution in the stand structure. By using flexible class boundaries with a fixed number of diameter classes, different forest structures can be simulated. An even-aged forest, for example, is simulated with a small diameter range between the smallest and largest classes. All classes will then effectively belong to the same stratum. An uneven-aged forest is simulated by applying a large range of number of individuals between the diameter classes. Different diameter classes will therefore effectively represent different strata. The limitations of this approach become apparent when the tree-ring width data and simulation are compared by calendar year as the model does not track individual trees.

Vegetation structure is then used for the calculation of the biophysical and biogeochemical processes of the model such as photosynthesis, plant hydraulic stress, and radiative transfer model. ORCHIDEE r5698 which is the version used in this study, combines the dynamic nitrogen cycle of ORCHIDEE r4999 (Vuichard et al., 2018; Zaehle & Friend, 2010) and the

explicit canopy representation of ORCHIDEE r4262 (Chen et al., 2016; Naudts et al., 2015; Ryder et al., 2016). It is one of the branches of the ORCHIDEE model and it was further developed, parameterized, and tested to simulate tree-ring widths.

In this study we use climate data from a gridded dataset developed for modelling, i.e., CRU-NCEP (Viovy, 2016), such that observed tree-ring widths can be used to evaluate the skill of the land-surface model ORCHIDEE r5698 to simulate radial tree growth. A description of ORCHIDEE-CN-CAN following Eq. 1 and detail the implementation of the ecophysiological processes that underlie the emerging capability of the model to simulate tree-ring widths is given in Text S1.

2. Description of ORCHIDEE in function of the aggregation model

2.1 Dependency of tree growth on climate

For deciduous trees, when the phenological thresholds are exceeded in ORCHIDEE r5698, leaves emerge using carbon from the reserve pool and as such an essential condition for carbon assimilation is fulfilled. Carbon assimilation is calculated following the analytical solution of the Farquhar and Ball and berry model, defined by Yin and Struik (Yin & Struik, 2009):

$$C_i = C_a - \mathrm{F}_A \times (1/g_b + 1/g_s)\,, \tag{1}$$

$$C_c = C_i - F_A/g_m\,, \tag{2}$$

$$F_A = {(C_c - \Gamma^*) \times x1}\Big/{(C_c + x2)} - F_{Rd}\,, \tag{3}$$

where C_i, C_a, and C_c are intercellular, inside of the canopy, and chloroplast CO_2 partial pressure, respectively (μbar), F_A is the rate of assimilation ($\mu mol\ CO_2 \cdot m^{-2} \cdot s^{-1}$), g_b, g_s,

and $g_m$are the boundary layer, stomatal, and mesophyll diffusion conductance ($mol \cdot m^{-2} \cdot s^{-1} \cdot bar^{-1}$), Γ^* is the CO_2 compensation point (μbar), $x1$ and $x2$ are the variables differ by the limitation for the assimilation (Rubisco-limited or electron-transport-limited), and F_{Rd} is the day respiration ($\mu mol\ CO_2 \cdot m^{-2} \cdot s^{-1}$). The assimilation is co-limited by stomatal conductance which accounts for plant hydraulic architecture (Sperry, Nichols, Sullivan, & Eastlack, 1994). Subsequently the newly assimilated carbon is stored in the labile pool. After satisfying the carbon cost of maintenance respiration (Amthor, 1984), the fraction of the labile pool that will be allocated to total biomass production (ΔM_{tot}) and the associated growth respiration are calculated as a function of temperature. The temperature dependency of plant growth (Fatichi, Leuzinger, & Körner, 2014) was accounted for as follows:

$$\Delta M_{labile\_c} = M_{labile\_c} + \Delta F_{gpp} \tag{4}$$

$$\Delta M_{tot\_c} = f_{gtemp} \times M_{labile\_c} \tag{5}$$

$$g_{temp} = f(T), \tag{6}$$

where M_{labile} is carbon mass of labile pool ($gC \cdot m^{-2}$), GPP is gross primary production ($gC \cdot m^{-2} \cdot dt^{-1}$), M_{tot} is total allocatable carbon ($gC \cdot m^{-2}$), f_{gtemp} is the turnover coefficient for the labile carbon pool (unitless), and T is the air temperature (K). f_{gtemp} increases with increasing long term annual mean temperature, but was set to never exceed 0.75.

As such photosynthesis (ΔF_{gpp}) and biomass production (M_{tot_c}) are no longer strictly coupled. This approach thus partly addresses the criticism that growth in most vegetation models is too strongly driven by photosynthesis (Fatichi et al., 2014). The dependency of tree-ring width on

climate thus emerges primarily from the control of radiation, temperature, and soil humidity on gross primary production (GPP), autotropic respiration, and biomass production.

2.2 Dependency of tree growth on tree age or size

The allocation scheme is based on the pipe model theory (Shinozaki, Yoda, Hozumi, & Kira, 1964) and its implementation by Sitch et al., (2003) and Magnani et al., (2000). The scheme allocates carbon to different biomass pools, e.g., leaves, fine roots, and sapwood, while respecting the differences in longevity and hydraulic conductivity between the pools (Naudts et al., 2015). According to the pipe model theory, each unit of branch and stem, a so-called pipe, supports a specific amount of leaves providing both mechanical and functional support. From this assumption, leaf mass (M_{l_c}; $gC \cdot tree^{-1}$), sapwood mass (M_{s_c}; $gC \cdot tree^{-1}$) and height (d_h; m) relate as follows:

$$M_{s\_c}/M_{l\_c} = d_h/f_{KF} \times k_{ff}. \tag{7}$$

Where f_{KF} (m) is defined as,

$$f_{KF} = k_{ls}/(k_{sla} \times k_{\rho s} \times k_{ff}), \tag{8}$$

where k_{sla} is the specific leaf area($m^2 gC^{-1}$), $k_{\rho s}$ is the sapwood density ($gC \cdot m^{-3}$), $k_{ff}$is the tree form factor indicating how the stem differs from a cylinder, and k_{ls} is the target leaf area to sapwood area ratio, which is calculated as:

$$k_{ls} = k_{lsmin} + f_{P_{gap}} \times (k_{lsmax} - k_{lsmin}), \tag{9}$$

where k_{lsmin} is the parameter from minimum observed leaf area to sapwood area ratio, $f_{P_{gap}}$ is a light stress factor based on the transmitted light (Haverd et al., 2012), and k_{lsmax} is the parameter from maximum observed leaf area to sapwood area ratio. Root mass and sapwood

mass are proportional to tree height to account for hydraulic constraints on, optimal growth (Magnani et al., 2000):

$$M_{s\_c}/M_{r\_c} = k_{sar} \times d_h \times k_{ff} \,, \tag{10}$$

where the variable k_{sar} (m^{-1}) represents the carbon cost to connect a root pipe to a sapwood pipe (Magnani et al., 2000):

$$k_{sar} = \sqrt{(k_{Cr}/k_{Cs}) \times (k_{\tau s}/k_{\tau r}) \times 2 \times k_{\rho s}/1000} \,, \tag{11}$$

where k_{Cr} is the conductivity of root $(m^3 \cdot kg^{-1} \cdot s^{-1} \cdot MPa^{-1})$, k_{Cs} is the conductivity of sapwood $(m^2 \cdot s^{-1} \cdot MPa^{-1})$, $k_{\tau s}$ is the sapwood longevity (days), and $k_{\tau r}$ is the root longevity (days). The multiplication by 2 converts carbon density into wood density and the division by 1000 converts g to kg. Following substitution of Eq. (10) in (7), a linear relationship of leaf mass and root mass is obtained:

$$M_{l\_c}/M_{r\_c} = f_{LF} \,, \tag{12}$$

where,

$$f_{LF} = k_{sar} \times f_{KF} \,. \tag{13}$$

Tree height is calculated using a relationship between tree height and basal area (d_{ba}) (Pretzsch, 2009):

$$d_h = k_{pipe2} \times \left(4/\pi \times d_{ba}\right)^{\frac{k_{pipe3}}{2}} \,, \tag{14}$$

where $pipe_2(m^{-1})$ and $pipe_3$(unitless) are parameters relating tree height and basal area. At the start of the allocation module, it is checked whether the current biomass pools satisfy the allometric relationships. Biomass pools are expected to be out of balance after carbon losses

through leaf, sapwood and root-specific turnover have been accounted for. If compared to the allometric relations there are imbalances in the biomass pools, newly assimilated carbon is used for restoring the allometric relationships. If some of the carbon is left from restoring, it will be allocated for growth while accounting for intra-stand competition. Tree-ring growth thus accounts for the pipe-model theory, allometric relationships and within-stand competition between diameter classes (Deleuze, Pain, Dhôte, & Hervé, 2004):

$$\Delta d_{ba(i)} = f_{\gamma} \times \left(d_{cir(i)} - k_m \cdot f_{\sigma} + \left(\left(k_m \times f_{\sigma} + d_{cir(i)}\right)^2 - 4 \times \sigma \times d_{cir(i)}\right)^{1/f_{power}}\right)/2 \,. \quad (15)$$

Where, f_{γ} is the variable that relates the d_{ba} increment of a tree to its d_{ba} . ORCHIDEE r5698 is not an individual-based model, and instead the model simulates stand structure by using a prescribed number of size classes (i index in equation 15). Therefore, $d_{cir(i)}$ denotes the circumference of size class i, and $\Delta d_{ba(i)}$ is a basal area increment of size class i which can be converted in tree-ring width increment if the diameter of the tree is known. In ORCHIDEE r5698, each diameter class represents trees with a different mean diameter and height and therefore informs the user about the social position of trees within the canopy. The difference in social position within a stand is the basis of intra-stand competition, which accounts for the fact that trees with a dominant position in the canopy are more likely to intercept light than suppressed trees and therefore contribute more to the stand-level photosynthesis and biomass growth (Deleuze et al., 2004). In Eq. 15, m is a smoothing parameter, σ is a circumference threshold for allocating carbon, and f_{power} is the denominator of power for deleuze-dhote simulation.

In the original equation, f_{power} is 2, which results in a linear increase in $\Delta d_{ba(i)}$ with $d_{cir(i)}$ (see Fig. 3 in Bellassen et al., (2010)). Following the observation that ecological properties such as crown length and tree height first increase but then saturate with an increasing diameter (Hemery, Savill, & Pryor, 2005; Peper, McPherson, & Mori, 2001), we introduced such a saturation point in the relationship between Δd_{ba} and d_{cir} by making f_{power} a function of the tree diameter:

$$f_{power} = 1.8 + k_{power} \times d_{dia}. \tag{16}$$

Where k_{power} is the slope for the f_{power} increment by d_{dia}. Following empirical testing, k_{power} was set such that f_{power} ranged between 2 and 3.5 as higher values further increase the similarity between the diameter classes, making their use meaningless.

According to Eq. 15, biomass is allocated to all size classes but more biomass will be allocated to the larger than to smaller size classes (see Fig. 3 in Bellassen et al., (2010)). Furthermore, the calculation of tree growth needs to conserve mass:

$$\Delta M_{tot\_c} = \sum_i (\Delta M_{c(i)} \times d_{ind(i)}), \tag{17}$$

$$\Delta M_{s\_c(i)} + \Delta M_{l\_c(i)} + \Delta M_{r\_c(i)} = \Delta M_{c(i)} . \tag{18}$$

Where $\Delta M_{c(i)}$, $d_{ind(i)}$, $\Delta M_{s\_c(i)}$, $\Delta M_{l\_c(i)}$, and $\Delta M_{r\_c(i)}$ are respectively, the total allocated carbon $(gC \cdot tree^{-1})$, the number of trees per meter square , and the increase of sapwood mass, leaf mass, root mass, in size class . $\Delta M_{s\_c(i)}, \Delta M_{l\_c(i)}, \Delta M_{r\_c(i)}$. The height increment can be re-written using Eqs. (7), (10), and (14):

$$(M_{s\_c(i)} + \Delta M_{s\_c(i)}) \Big/ (M_{l\_c(i)} + \Delta M_{l\_c(i)}) = (d_{h(i)} + \Delta d_{h(i)}) \Big/ f_{KF} \times k_{FF} , \tag{19}$$

$$(M_{s\_c(i)} + \Delta M_{s\_c(i)}) \Big/ (M_{r\_c(i)} + \Delta M_{r\_c(i)}) = k_{sar} \times (d_{h(i)} + \Delta d_{h(i)}) \times k_{FF} \,, \tag{20}$$

$$d_{h(i)} + \Delta d_{h(i)} = k_{pipe2} \times \left({}^{4}/_{\pi} \times (d_{ba(i)} + \Delta d_{ba(i)})\right)^{\frac{k_{pipe3}}{2}} . \tag{21}$$

Subsequently, Eqs. (17) to (21) need to be solved simultaneously to obtain a value for k_γ to deteremine $\Delta M_{s\_c(i)}$, $\Delta M_{l\_c(i)}$, $\Delta M_{r\_c(i)}$, $\Delta d_{h(i)}$, and $\Delta d_{ba(i)}$. In other words, a value for f_γ needs to be found that both satisfies the allometric relationships and also conserves mass. Such the system of equations cannot be solved analytically and would require an iterative scheme. ORCHIDEE r5698, however, overcomes the need for iterations by assuming a locally linear relationship of height and basal area (linearization of Eq. (14)). The fact that the calculation is performed at daily time steps makes this a fair assumption because the height increment during a single day is small:

$$\Delta d_{h(i)} = \Delta d_{ba(i)} / f_{s(i)} \,, \tag{22}$$

where, $f_{s(i)}$ is the slope of the linear relationship between a small increment in height and basal area. Eq. (21) can therefore be re-rewritten as:

$$f_{s(i)} = \frac{\Delta d_{ba(i)}}{\mathrm{k_{pipe2}} \times \left({}^{4}/_{\pi} \times \left(\mathrm{d}_{ba(i)} + \Delta d_{ba(i)}\right)\right)^{k_{pipe3}/2} - k_{\mathrm{pipe2}} \times \left({}^{4}/_{\pi} \times \mathrm{d}_{ba(i)}\right)^{k_{pipe3}/2}} \tag{23}$$

where $\Delta d_{ba(i)}$ is a small increment of basal area of size class i.

By making use of f_s and the allometric relationship:

$$M_{s\_c(i)} + \Delta M_{s\_c(i)} + M_{h\_c(i)} = k_{ff} \times k_\rho \times \left(d_{ba(i)} + \Delta d_{ba(i)}\right) \times \left(d_{h(i)} + \Delta d_{h(i)}\right) \tag{24}$$

,where $M_{h\_c(i)}$ is the heartwood mass ($gC \cdot tree^{-1}$), $\Delta M_{s\_c(i)}$, $\Delta M_{l\_c(i)}$, and $\Delta M_{r\_c(i)}$ are then calculated by:

$$\Delta M_{s\_c(i)} = k_{ff} \times k_{\rho} \times \left(d_{ba(i)} + f_{I(i)} \times f_{\gamma}\right) \times \left(d_{h(i)} + {f_{I(i)}}/{f_s} \times f_{\gamma}\right) - M_{s\_c(i)} - M_{h\_c(i)}, \tag{25}$$

$$\Delta M_{l\_c(i)} = f_{KF} \times k_{ff} \times k_{\rho} \times \left(d_{ba(i)} + f_{I(i)} \times f_{\gamma}\right) - (f_{KF} \times M_{h\_c(i)})/(d_{h(i)} + {f_{I(i)}}/{f_{s(i)}} \times f_{\gamma}) - M_{l\_c(i)}, \tag{26}$$

$$\Delta M_{r\_c(i)} = {f_{KF}}/{f_{LF}} \times k_{ff} \times k_{\rho} \times \left(d_{ba(i)} + f_{I(i)} \times f_{\gamma}\right) - ({f_{KF}}/{f_{LF}} \times M_{h\_c(i)})/(d_{h(i)} + {f_{I(i)}}/{f_{s(i)}} \times f_{\gamma}) - M_{r\_c(i)}, \tag{27}$$

where k_{ρ} is wood density ($gC \cdot m^{-3}$) and $f_{I(i)}$ is part of Eq. 15

$$\left(d_{cir(i)} - k_m \cdot f_{\sigma} + \left(\left(k_m \times f_{\sigma} + d_{cir(i)}\right)^2 - 4 \times \sigma \times d_{cir(i)}\right)^{1/f_{power}}\right)/2 \tag{28}$$

When substituting Eq. (24), (25) and (26) in Eq. (17), a quadratic equation for f_{γ} is obtained. Subsequently the increase in tree-ring width for each diameter class is calculated by using the positive root of f_{γ} in Eq. (15). The size-related decrease in tree-ring width, which could be as much as one order of magnitude, thus emerges from simulating wood growth following allometric relationships under the assumption that a certain mass of sap wood is required to support root and leaves for mechanical and functional support (Magnani et al., 2000; Shinozaki et al., 1964).

2.3 Dependency of tree growth on endogenous disturbances

The endogenous disturbances that are accounted for correspond to self-thinning, recruitment and background mortality. Self-thinning takes place in an overcrowded stand due to resource competition such as light, soil water, and nutrient. When the resource supply is insufficient, the density of a stand starts to decrease, a process known as self-thinning. In ORCHIDEE we thus use a pre-defined self-thinning relationship that reflects the maximum possible density of a stand at a given tree size. Tree size has been quantified by biomass, diameter, volume, and height (Reineke, 1933; Zeide, 2010) as described in the previous section. In ORCHIDEE r5698, a relationship between number of individuals and the quadratic mean diameter is used to define the self-thinning relationship:

$$d_{ind\_max} = {d_{dia}}\Big/{k_{\alpha\_s}}^{1/k_{\beta\_s}}, \tag{29}$$

where d_{ind_max} is the number of individual per hectare from the self-thinning relationship $(trees \cdot m^{-2})$, d_{dia} is the quadratic mean diameter (m) across all size classes, k_{α_s} is the intercept for the self-thinning relationship, and k_{β_s} is the slope for the self-thinning relationship. At the start of a simulation, the initial number of individuals is prescribed to overcome numerical issues from the self-thinning relationship stemming from the fact that this relationship is ill-defined for very small trees. The loss of trees by self-thinning starts when d_{ind_max} calculated from the self-thinning relationship is smaller than the actual number of individuals in the model (d_{ind}). If this is the case d_{ind} is set to d_{ind_max} and $d_{ind} - d_{ind\_max}$ trees are killed.

Recruitment occurs when resources are underused. In ORCHIDEE r5698, the number of recruits is calculated as a function of the light availability at the forest floor (Rüger, Huth, Hubbell, & Condit, 2009):

$$\log_{10} d_{ind\_new} = k_{\alpha\_r} + k_{\beta\_r} \times (\log_{10}(f_L + \epsilon) - k_{\bar{L}}), \quad (30)$$

Where d_{ind_new} is the number of recruits added per m^2 area $(trees \cdot m^{-2})$, k_{α_r} is the intercept, k_{β_r} is the slope for the relationship that links the number of recruits to the available light, f_L is the seasonal average of the transmitted light that reaches to the floor, ϵ is a small offset added to avoid taking the log of zero (10E-8), and $k_{\bar{L}}$ is an average of the $\log_{10}$ light that ensures that recruitment only occurs if the seasonal mean transmittance exceeds the average transmittance. The calculation is done at the end of each year and only for PFTs where recruitment is expected to be substantial and therefore accounted for. The calculated recruits are added to the smallest size class.

Background mortality represents the loss of individuals in stands in the absence of self-thinning when the stand is young. It, thus, represents individual tree mortality that is unexplained from the endogenous and exogenous disturbances accounted for in ORCHIDEE. Background mortality is calculated using a concept of residence time for a tree and it is a constant-low rate of tree mortality that is applied to the living biomass.

$$k_{fdeath} = 1/k_{\tau\_res}, \quad (31)$$

where k_{fdeath} is the mortality (day^{-1}), and k_{τ_res} is the residence time $(days)$. If mortality from self-thinning occurs, background mortality is not accounted for because self-thinning and background mortality would not be independent when the stand is matured. This implies that only the population dynamics of young stands are governed by background rather than self-thinning mortality. The within-stand population dynamics described above control the contribution of endogenous disturbances to tree growth.

2.4 Dependency of tree growth on exogenous disturbances

The main exogenous disturbances in forests are fire, pests, droughts, windthrow (Seidl et al., 2017), management (Pichler, Godinho-Ferreira, Zlatanov, Pichlerová, & Gregor, 2010), N-deposition (Vitousek et al., 1997), and CO_2 fertilization (Schimel, 1995). Except for pests, all is included in ORCHIDEE r5698, but only the latter three were implemented such that they affect the simulated tree-ring width.

One of the biggest exogenous disturbances, affecting 98% of the European forest and over 50% of the global forests, is forest management (Pichler et al., 2010). ORCHIDEE r5698 simulates four management strategies: (1) unmanaged stands of which mortality is driven solely by self-thinning, (2) regular thinning and harvesting of wood, (3) coppicing, and (4) short rotation coppicing of willow and poplar for biomass production (Naudts et al., 2015). Under all three management systems a harvest is triggered when a PFT and management-specific maximum diameter or minimum stand densities is exceeded. Under thin and fell management thinning makes use of the concept of relative density index (f_{RDI}) (Bellassen et al., 2010) and aims at reducing resource competition for the remaining individuals:

$$f_{RDI} = {d_{ind}}/{d_{ind\_max}}\,, \tag{32}$$

where d_{ind_max} is the maximum number of individuals from self-thinning relationship ($trees \cdot m^{-2}$).

The global nitrogen cycle has been strongly perturbed by anthropogenic activities (Vitousek et al., 1997); biologically reactive nitrogen is emitted to the atmosphere (Durka, Schulze, Gebauer, & Voerkeliust, 1994) and has caused an increase in the biological carbon sequestration following wet and dry deposition especially in the context of increasing atmospheric CO2 concentration given that nitrogen availability may become a limiting factor (Bowman &

Steltzer, 1998; Janssens et al., 2010; Magnani et al., 2007). When the soil becomes nitrogen saturated negative effects on plant growth, soil fertility, and water quality have been observed (Aber et al., 1998). ORCHIDEE r5698 includes a dynamic nitrogen cycle and thus accounts for plant responses and tree ring growth to nitrogen deposition and nitrogen limitation.

The nitrogen cycle in ORCHIDEE r5698 follows the approach implemented in an earlier version of ORCHIDEE (Zaehle & Friend, 2010) and the enhancements proposed in ORCHIDEE r4999 (Vuichard et al., 2019). At every time step, ORCHIDEE r5698 reads the total nitrogen deposition from a nitrogen input file which prescribes four nitrogen sources: deposition of ammonium, deposition of nitrate, fertilization and biological nitrogen fixation. Nitrogen losses through leaching resulting from drainage and gaseous emission resulting from nitrification and denitrification are accounted for. Furthermore, the plant-available nitrogen pool in the soil distinguishes an ammonium and nitrate pool which in turn depend on the abovementioned nitrogen inputs and outputs, as well as on the decomposition of litter and nitrogen immobilization. Nitrogen uptake by the plant depends on the plant-available nitrogen in the soil along with fine root mass (M_r), temperature and the actual plant nitrogen status. The nitrogen status of the plant is quantified through the dynamic C/N ratio of the leaves, roots, fruits, and the sapwood.

The nitrogen uptake is added to the labile pool before it is used in support of plant growth and it is allocated to the different biomass pools. In ORCHIDEE, nitrogen allocation follows carbon allocation:

$$\Delta M_{tot\_n} = f_{cost} \times f_{dnc} \times f_{nc\_l} \times f_{f\_R} \times \Delta M_{tot\_c}, \tag{33}$$

where ΔM_{tot_n} $(gN \cdot m^{-2})$ is nitrogen allocated to leaf, wood, root and fruits, f_{cost} is the nitrogen cost per unit carbon allocation and accounts for the differences in carbon-nitrogen

ratio between leaves, wood, root, and fruit, f_{dnc} is an elasticity parameter (Eq. (21) in Text S1 from (Zaehle & Friend, 2010)), f_{nc_l} is nitrogen-carbon ratio of leaf, and f_{f_R} is the fraction of the total allocatable carbon used for growth respiration. f_{cost} is calculated using the fraction of carbon allocated to leaves, wood, roots, and fruits on the basis of the carbon-nitrogen ratio of each compartment (Eq. (20) in Text S1 from (Zaehle & Friend, 2010)). f_{nc_l} dynamically dampens the nitrogen cost in accordance with the nitrogen available in the labile pool and the required nitrogen (ΔM_{tot_n}). In extreme cases where the nitrogen in the labile pool is not sufficient to sustain the growth in Eq. 32 and the maximum C/N ratio is reached, the nitrogen concentration of newly grown leaf is adjusted. The nitrogen concentrations in the leaves affect carbon dynamics through nitrogen-dependencies of maximum carboxylation capacity, electron transport capacity and maintenance respiration. Nitrogen availability will thus leave an imprint on the simulated tree-ring width.

Increased atmospheric CO_2 concentrations may now be among the most dominant anthropogenic disturbance. CO_2 fertilization stems from the fact that CO_2 may be a limiting factor for growth and thus increasing it could enhance plant growth. The effect has been examined through experiments (Ainsworth & Long, 2004) and tree-ring width observations (Cienciala et al., 2018; Koutavas, 2008), but the evidence from tree-ring records has been questioned (Brienen, Gloor, & Zuidema, 2012; Groenendijk et al., 2015). Assessing the response of trees to increasing atmospheric CO_2 concentrations is important for understanding changes in the global carbon cycle, consequently, numerous modelling approaches have been developed to simulate the CO_2 fertilization effect on net primary productions (Rathgeber et al., 2000; Su, Sang, Wang, & Ma, 2007) or tree-ring widths (Gaucherel, Guiot, & Misson, 2008; Li, Harrison, Prentice, & Falster, 2014). ORCHIDEE-CN-CAN prescribes atmospheric CO_2 concentrations based on reconstructions and observations. This input enables the model to

simulate responses of plant growth to increasing CO_2 concentrations following Eq. 1 to 3. Increased partial pressure of ambient CO_2 strengthens the cellular gradient in CO_2 which in turn results in greater assimilation in the model.

Current ORCHIDEE r5698 simulates the growth response to windthrow and drought. Critical wind speeds above which uprooting and stem breakage occurs are calculated as a function of tree dimensions and stand characteristics (Chen et al., 2018; Hale et al., 2015). Following wind damage, individual trees are killed. Following mortality from windthrow, ORCHIDEE r5698 grows new cohorts for the same PFT as before windthrow. This implies that ORCHIDEE does not simulate resource competition with existing cohorts, and therefore only represents stand-replacing disturbances from windthrow. Windthrow of a few individual trees within a stand would stimulate recruitment and therefore impact tree-ring with in real forests, but this chain of events is not simulated in ORCHIDEE r5698. In addition, windthrow which does not completely destroy a tree can impact tree ring growth; this process is also neglected in ORCHIDEE. The effect of windthrow on tree ring widths is therefore not accounted for at the moment.

Drought is defined by the 'absence of rainfall for a long enough period of time to result in depletion of soil water and injury to plants' (Kramer & Boyer, 1995). In ORCHIDEE r5698, based on aforementioned definition, drought is induced by the climate forcing. A hydraulic-based framework based on stomatal regulation (McDowell et al., 2008) has been implemented (Naudts et al., 2015) to simulate survival and mortality of plants from droughts. Drought-induced growth reduction is triggered by reduction in carbon assimilation and reflected in the tree-ring widths in the model. Referring to the hydraulic-based framework, there are two causes of mortality following a long and/or intense drought: carbon starvation which is caused by

carbon deficiency from stomata closure and hydraulic failure which comes from cavitation of xylem by the reduced water supply (Sevanto, McDowell, Dickman, Pangle, & Pockman, 2014). ORCDHIEE r5698 can simulate carbon starvation. Although ORCHIDEE r5698 simulates cavitation, it does not yet result in plant mortality.

Supplementary tables

Table S1. Description of the variables used in the description of the ORCHIDEE model

Name	Name in ORCHIDEE	Unit	Description
C_a	Ca	μbar	Inside canopy CO_2 partial pressure
C_c	Cc	μbar	Cholorplast CO2 partial pressure
C_i	$leaf\_ci$	μbar	Intercellular CO2 partial pressure
d_{ba}	ba	$m^2 \cdot tree^{-1}$	Plant basal area
d_{cir}	$circ\_class\_circ\_eff$	m	Effective circumference of individual trees
d_{dia}	Dg	m	Quadratic mean of diameter
d_h	$height$	m	Plant height
d_{ind}	$circ\_class\_n$	$trees \cdot m^{-2}$	Number of individuals in stand
d_{ind_new}	new_ind	$trees \cdot m^{-2}$	number of recruitments added
d_{ind_max}	$Nmax$	$trees \cdot hactare^{-1}$	Maximum number of trees according to the self-thinning relationship
F_A	$assimtot$	$\mu mol \cdot m^{-2} \cdot s^{-1}$	Carbon assimilation rate
F_{gpp}	gpp	$gC \cdot m^{-2} \cdot dt^{-1}$	Gross primary production
F_{Rd}	Rd	$\mu mol \cdot m^{-2} \cdot s^{-1}$	Respiratory CO2 release other than by photorespiration
f_{cost}	$costf$	-	Nitrogen cost per unit gram carbon
f_{dnc}	$1/deltacn$	-	

f_{f_R}	$1 - frac\_growthresp\_dyn$	-	Fraction of growth respiration usage from gross primary production
f_{gtemp}	$gtemp$	-	Turnover coefficient of labile carbon pool
f_{γ}	$gammas$	-	Slope for size competition
f_{KF}	KF	m	Scaling factor to convert plant sap wood mass to plant leaf mass
f_L	$lstress\_fac$	-	Fraction of light transmitted to the forest floor
f_{nc_l}	$1/cn\_leaf$	-	Nitrogen to carbon ration of leaf
f_{LF}	LF	-	Scaling factor to convert plant root mass to plant leaf mass
f_{Pgap}	$Pgap$	-	Transmission probability of light through to forest floor
f_{power}	$deleuze\_power$	-	
f_{RDI}	rdi	-	Relative density index
f_s	s	-	Slope of relationship between small increase of height and basal area
f_{σ}	$sigma$	-	Size threshold of plants for carbon allocation in size competition
g_b	gb_co2	$\mu mol \cdot m^{-2} \cdot s^{-1} \cdot bar^{-1}$	Boundary-layer conductance

g_m	gm	$\mu mol \cdot m^{-2} \cdot s^{-1} \cdot bar^{-1}$	Mesophyll diffusion conductance
g_s	gs	$\mu mol \cdot m^{-2} \cdot s^{-1}$	Stomatal conductance to CO2
k_{α_r}	$alpha\_recruitment$	-	Intercept for calculating new individuals from recruitments
k_{α_s}	$alpha\_selfthinning$	-	Intercept for the self-thinning relationship
k_{β_r}	$beta\_recruitment$	-	Slope for calculating new individuals from recruitments
k_{β_s}	$beta\_selfthinning$	-	Slope for the self-thinning relationship
k_{Cr}	k_root	$m^3 \cdot kg^{-1} \cdot s^{-1} \cdot MPa^{-1}$	Root specific conductivity
k_{Cs}	k_sap	$m^2 \cdot s^{-1} \cdot MPa^{-1}$	Sapwood specific conductivity
k_{fdeath}	$mortality$	$year^{-1}$	Background mortality
k_{ff}	$tree\_ff$	-	Tree form factor
$k_{\bar{L}}$	$\log_{10} 0.02$	-	Average log light
k_{ls}	k_latosa	-	Leaf area to sapwood area ratio
k_{lsmax}	k_latosa_max	-	Maximum leaf area to sapwood area ratio

k_{lsmin}	k_latosa_min	-	Minimum leaf area to sapwood area ratio
k_m	m_dv	-	Smoothing parameter for competition-allocation scheme
k_{pipe2}	$pipe\_tune2$	m^{-1}	Allometric parameter relating tree height and basal area
k_{pipe3}	$pipe\_tune3$	m	Allometric parameter relating tree height and basal area
k_{power}			
k_ρ	$pipe\_density$	$gC \cdot m^{-3}$	Wood density
$k_{\rho s}$	$sapwood\_density$	$mgC \cdot m^{-3}$	Sapwood density
k_{sar}	$c0\_alloc$	m^{-1}	Scaling factor to convert root mass to sapwood mass
k_{sla}	sla	$m^2 \cdot gC^{-1}$	Specific leaf area
$k_{\tau r}$	tau_root	$days$	Root longevity
$k_{\tau s}$	tau_sap	$days$	Sapwood longevity
k_{τ_res}	$residence\_time$	$years$	Residence time of plants
M_{h_c}	Ch	$gC \cdot tree^{-1}$	Plant heart wood mass
M_{l_c}	Cl	$gC \cdot tree^{-1}$	Plant leaf mass
M_{labile_c}	$labile\_pool$	$gC \cdot m^{-2}$	Carbon mass of labile pool
M_{r_c}	Cr	$gC \cdot tree^{-1}$	Plant root mass
M_{s_c}	Cs	$gC \cdot tree^{-1}$	Plant sap wood mass
ΔM_{tot_n}	n_alloc_tot	$gN \cdot m^{-2}$	Nitrogen growth
M_{tot_c}	$circ\_class\_biomass$	$gC \cdot tree^{-1}$	Plant total biomass

T_{2m}	$t2m$	K	Air temperature at 2m
$x1$	$x1$	$\mu mol \cdot m^{-2} \cdot s^{-1}$	The variable to solve analytic equation for assimilation.
$x2$	$x2$	μbar	The variable to solve analytic equation for assimilation.
ϵ	min $\_stomate$	-	Small value to avoid numerical problems
Γ^*	$gamma\_star$	μbar	CO2 compensation point

Table S2. Characteristics of the proposed benchmarks. These benchmarks were designed to better constrain physiological and ecological processes in land-surface models. Given their intended use with ITRDB data, the benchmarks had to propose solutions for well-known issues of the ITRDB.

Benchmark	Metrics	Targeted process understanding	Solutions for meaningful model comparison with ITRDB	Figure
Size dependent growth	· RMSE · Slope of the residuals	· Long-term size-related growth · Within-stand competition	· Select the biggest tree of the simulation · Construct an average virtual tree aligned by tree age	Fig. 4
Diameter increment of mature trees	· RMSE · Slope of the residuals	· Long-term tree growth after establishment · Within-stand competition	· Select the biggest tree of the simulation · Construct an average virtual tree aligned by calendar year	Fig. 5
Diameter increment of young trees	· RMSE · Slope of the residuals	· Short-term (i.e. 30-year) tree growth during establishment · Size-related growth	· Select the biggest tree of the simulation · Construct a fast-growing virtual tree	Fig. 6
Extreme growth	· Extreme events · Amplitude	· Yearly climate sensitivity	· Select the biggest tree of the simulation · Define extreme growth using 25% smallest and 75% largest observations	Fig. 7

Table S3. Information of the sites used in the test.

Site code in BACI	Longitude	Latitude	Management	Number of individual series	Length of longest individual record (years)
DEO	46.81	9.46	Y	61	248
DVN	46.82	9.86	Y	97	208
GIU	47.44	25.46	N	116	90
HD2	49.19	19.90	N	64	258
SCH	46.69	7.26	Y	158	188
SOB	46.73	9.48	Y	78	188
TIC	49.22	19.98	N	104	165
CAN	46.07	12.37	N	120	145
SOR	55.42	11.59	Y	53	88
TER	42.49	13.00	N	98	333
ZOF	47.30	7.96	N	61	156

355 **Supplementary figure**

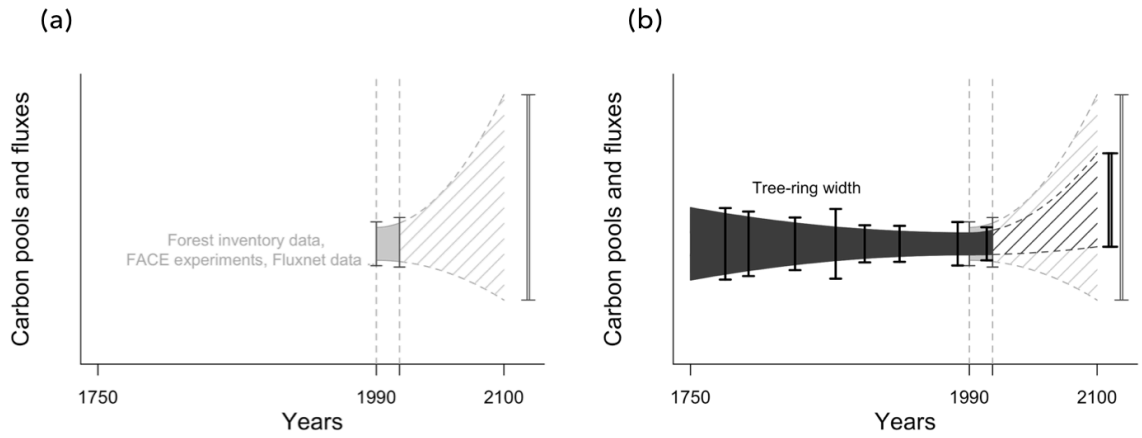

356

357 **Figure S1. Conceptual illustration of the expected reduction in model uncertainty**
358 **following the use of tree-ring width records to benchmark land-surface models.** Note that
359 the anticipated uncertainty reduction assumes that a large part of the model uncertainty comes
360 from the model formulation and its parameters rather than from the initial conditions and
361 drivers. (a) Observational constraints (grey vertical bars) from short-term benchmarks such as
362 forest inventory data, FACE experiments, and FLUXNET data, have been used to parameterize
363 and evaluate the response of ecosystems to environmental changes (light-grey coloured area).
364 When used in projecting the present-day to future carbon pools and fluxes, uncertainty in
365 ecosystem response to climate change is propagated through the model resulting in
366 unacceptably large uncertainties (light-grey hatched area). (b) Tree-ring records going back to
367 pre-industrial times (black vertical bars) are expected to better constrain the response of
368 ecosystems to environmental changes (dark-grey coloured area) which should result in smaller
369 uncertainties when used to project future ecosystem responses (dark-grey hatched area).

370

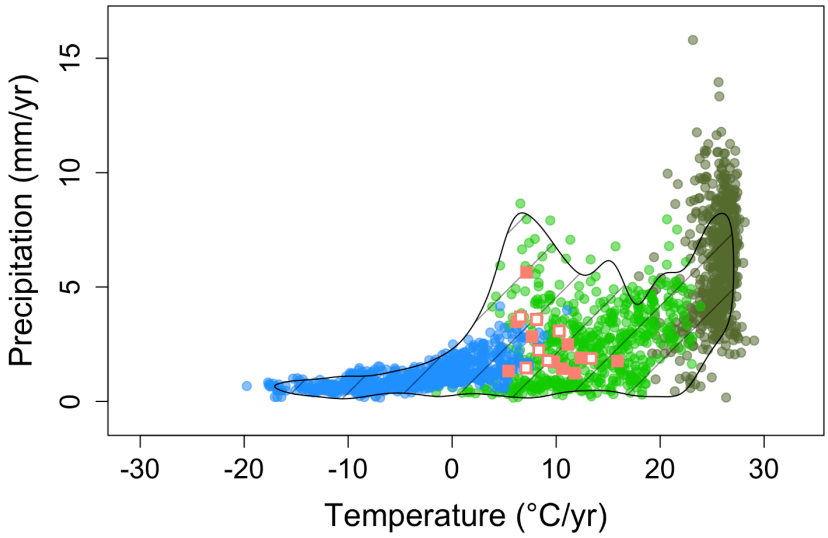

Figure S2. Distribution of the ITRDB and European network data in climate space. The circles denote the distribution of forests based on the land cover map of the ORCHIDEE model in the year 2000 (Poulter et al., 2015). Tropical forests are shown in dark green, temperate forests in light green and boreal forests in blue. Hatching shows the distribution of ITRDB sites which covers except for the wet tropics almost the entire climatic range of forests. The pink square points show the distribution of the European biomass network and the sites used in this study are presented as white square points. All annual temperature and precipitation are based on CRU-NCEP data for the year 2000 (Viovy, 2016).

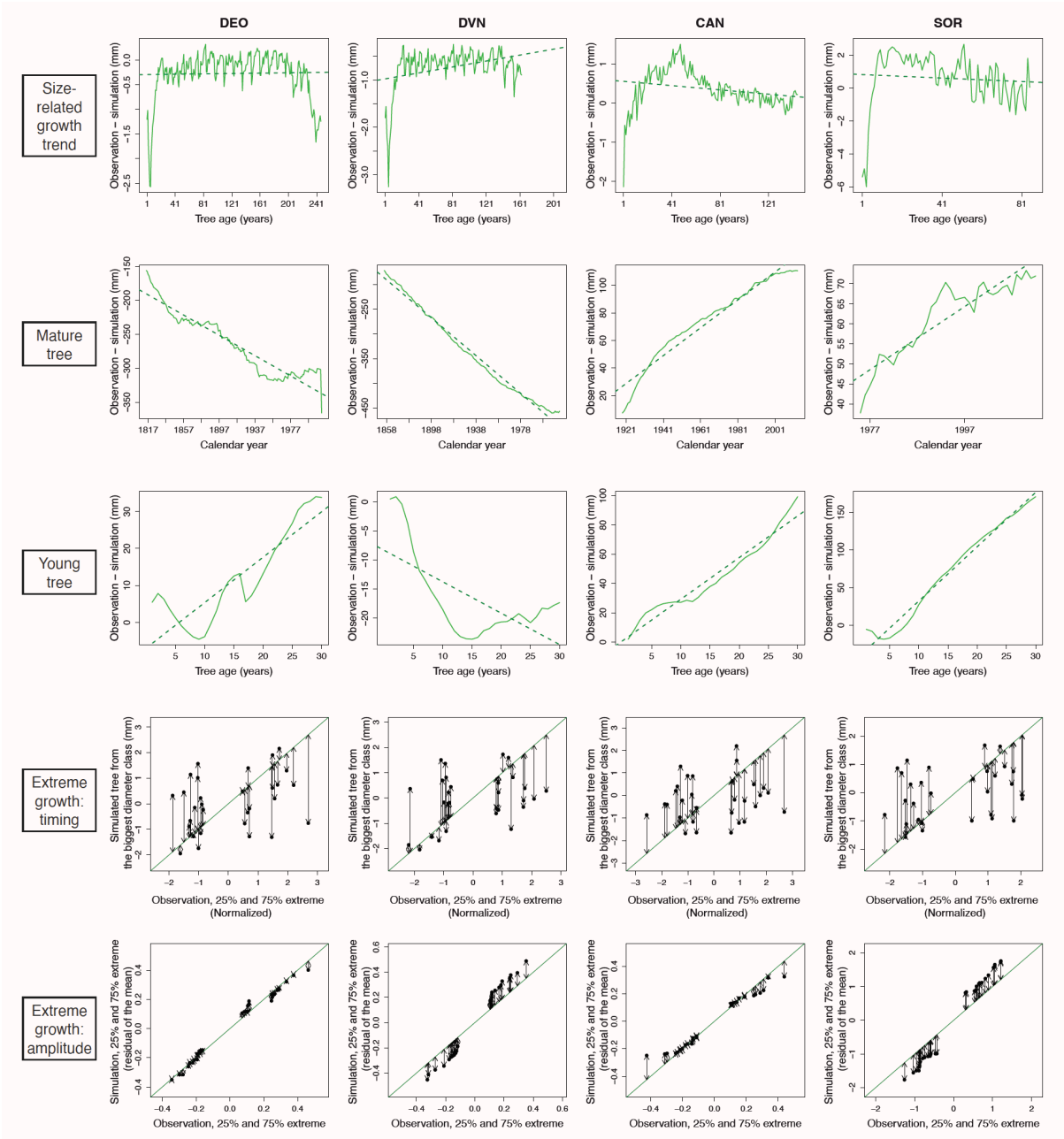

Figure S3. Details of the four benchmarks for four out of the 11 sites selected from the European biomass network. Each column denotes a single site. The DEO and DVN represent Norway spruce forests. The CAN and SOR sites are Beech forest. Each row denotes a different benchmark. The first row corresponds to the benchmark explained in Fig. 5 d, the second row to Fig. 6 f, the third row to Fig. 7 f, and the fourth and fifth rows to Fig. 8 d and f, respectively. In the first three rows, the green line denotes the model residuals, and the green dotted line is the linear regression of the model residuals. In the fourth and the fifth

row, the green line presents a 1:1 line, and the black arrow shows the distance between the 1:1 line and each point. See section 2.4 for details.

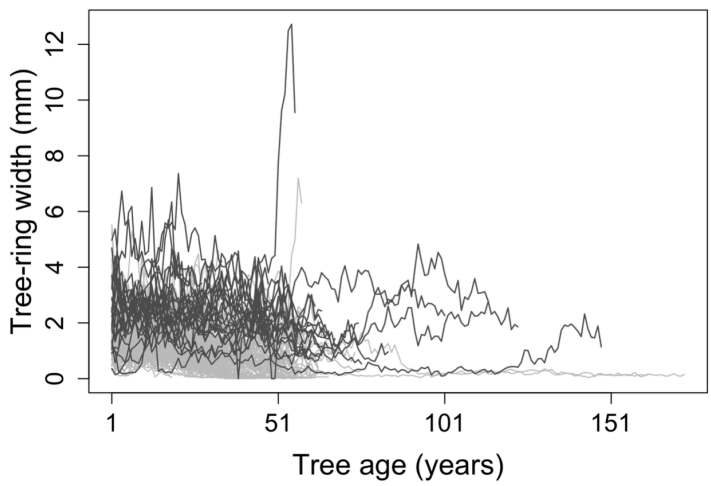

Figure S4. TRW at the SCH site. Individual lines represent each tree in the dataset, and dark-grey lines represent the 15% biggest trees that were selected for the big-tree sample. Note that the two oldest trees, which are about 40 years older than other trees, were not retained for the big tree sample. The presence of these two trees in the all tree sample but their absence in the big tree sample is responsible for a large difference (more than 1 mm) in the tree-ring width of the virtual tree. Large differences between the virtual tree for the unbiased and large-tree sample may result in different outcomes for the optimization.

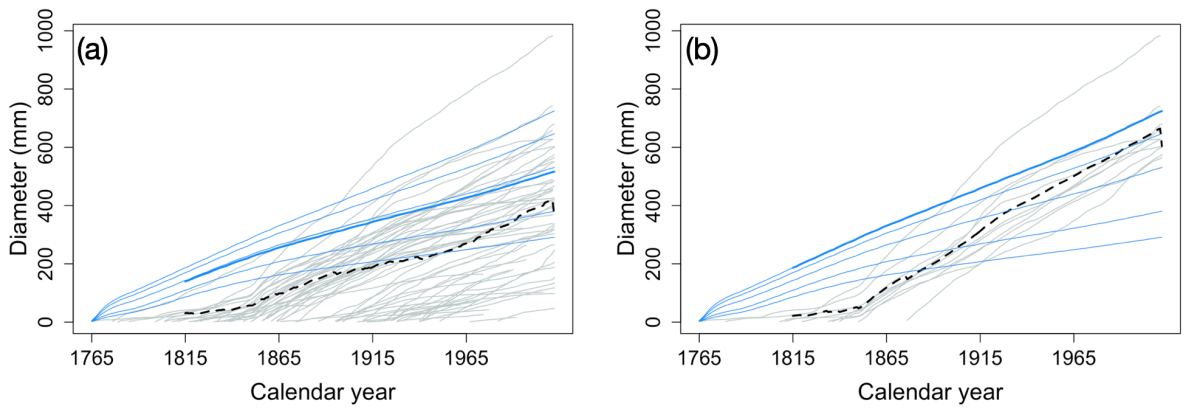

Figure S5. TRW at the DEO site. (a) Observed TRW is shown as grey lines, whereas the simulations are shown in blue. The growth trend of a mean virtual tree from whole simulation (blue bold line) and whole observation (black dotted line) are similar to each other, however, (b) the observed growth trend becomes much steeper than the simulated trend if only the big trees were sampled. Large differences between the virtual tree for the unbiased and large-tree sample may result in different outcomes for the optimization.

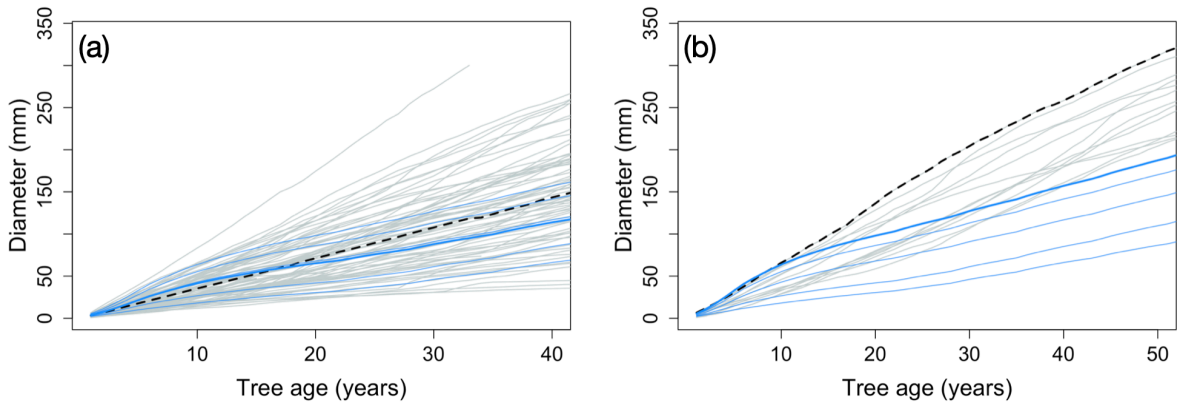

Figure S6. TRW at the SOB site. (a) Observed TRW is shown as grey lines, whereas the simulations are shown in blue. This figure presents the all-tree data; the mean simulation (bold blue line) and the observed mean growth (black dotted line), respectively. Note that for the unbiased sample the mean simulation and virtual tree are close to each other. (b) The big-tree data is shown in grey. For big-trees, the simulation of the largest diameter class (bold blue line) and the yearly maximum growth of the virtual tree (black dotted line) are very different. Large differences between the virtual tree for the unbiased and large-tree sample may result in different outcomes for the optimization.

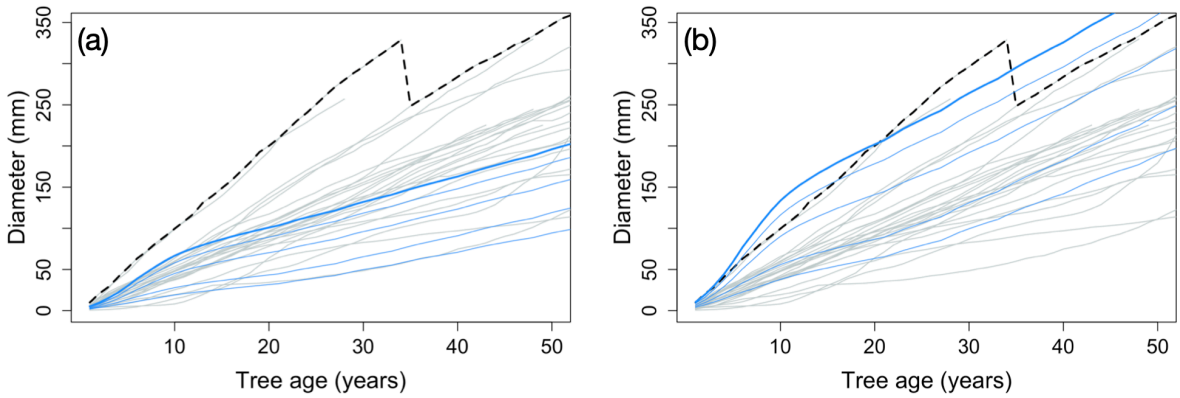

Figure S7. TRW at the SCH site. (a) Big-trees data (grey) and simulations (blue) before arithmetic optimization. (b) Big-trees data and simulations after applying the multiplier that minimizes RMSE between the largest simulated diameter class (blue bold line) and virtual tree (black dotted line). Since two trees grew much faster than the other trees and they grow fast enough to belong to the top 15% big-trees, the optimized simulations largely overestimate the overall growth.

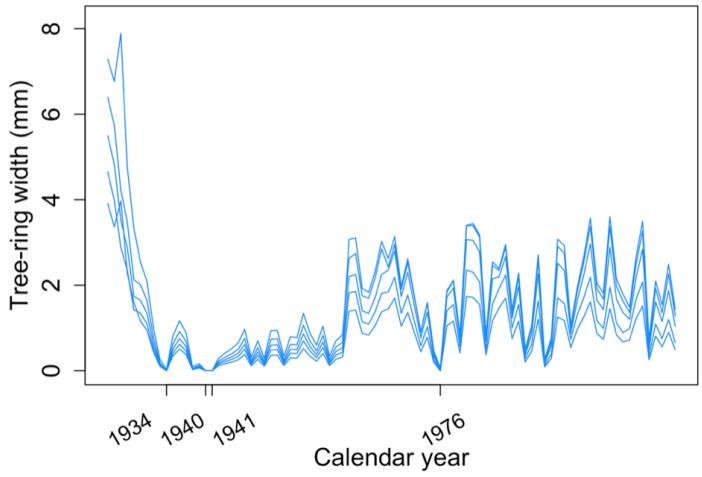

Figure S8. The Simulated tree-ring widths for the site SOR. ORCHIDEE simulated zero-growth for 4-years: 1934, 1940, 1941, and 1976. Note that 1976 was an extreme drought year in Denmark were the site is located.

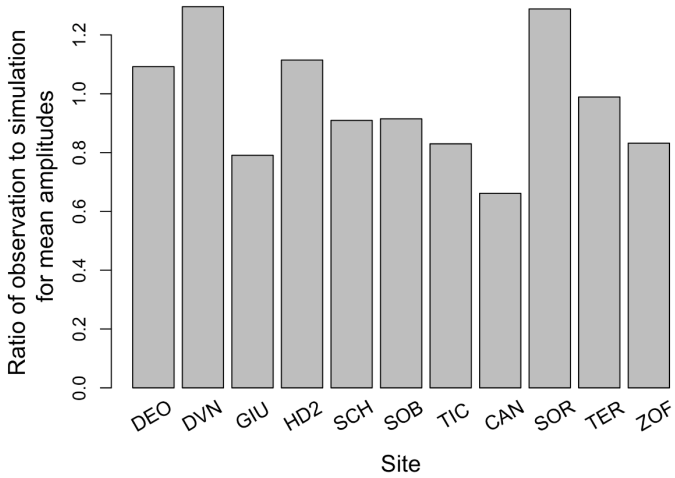

Figure S9. Ratio of the observed to simulated mean amplitudes.

Ratio of the observed to simulated mean amplitudes. The ratio is calculated as the ratio of the interquartile range in observations divided by the interquartile range in simulations. A ratio of 1 indicates that the observed variation is equal to that of simulations; with a ratio larger (smaller) than 1 indicating the observed variation is larger (smaller) than simulated. Site DVN showed the biggest number.

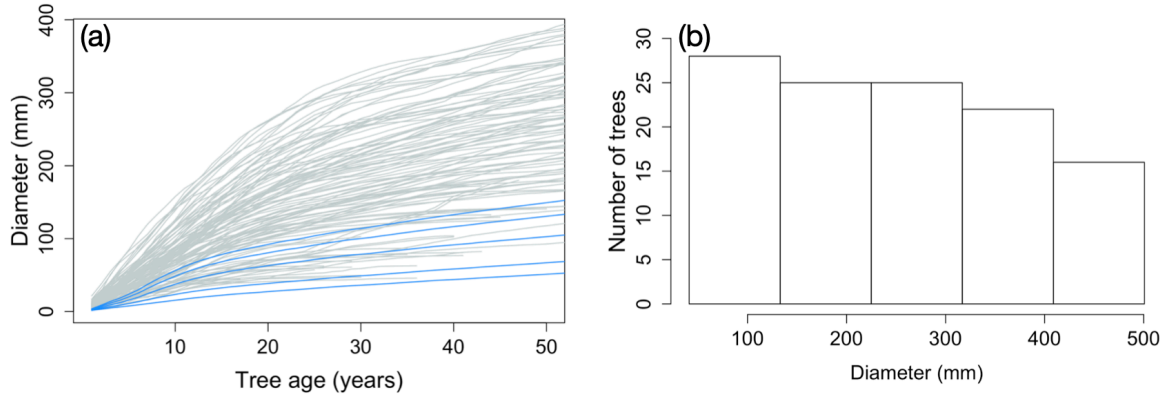

Figure S10. TRW at the GIU site. (a) Observed TRW is shown as grey lines, whereas the simulations are shown in blue. The TRW at the site GIU was not reproduced well. (b) The stand structure of the observation is different from the simulation of which is distributed 15, 21, 27, 21, 15 % of the total number of trees from the smallest to the largest size classes.

References

Aber, J., McDowell, W., Nadelhoffer, K., Magill, A., Berntson, G., Kamakea, M., … Fernandez, I. (1998). Nitrogen saturation in temperate forest ecosystems. *BioScience*, *48*(11), 921–934. https://doi.org/10.2307/1313296

Ainsworth, E. A., & Long, S. P. (2004). What have we learned from 15 years of free-air CO2 enrichment (FACE)? A meta-analytic review of the responses of photosynthesis, canopy properties and plant production to rising CO2. *New Phytologist*, *165*(2), 351–372. https://doi.org/10.1111/j.1469-8137.2004.01224.x

Amthor, J. S. (1984). The role of maintenance respiration in plant growth. *Plant, Cell and Environment*, *7*(8), 561–569. https://doi.org/10.1111/1365-3040.ep11591833

Bellassen, V., Le Maire, G., Dhôte, J. F., Ciais, P., & Viovy, N. (2010). Modelling forest management within a global vegetation model—Part 1: Model structure and general behaviour. *Ecological Modelling*, *221*(20), 2458–2474. https://doi.org/10.1016/j.ecolmodel.2010.07.008

Bowman, W. D., & Steltzer, H. (1998). Positive feedbacks to anthropogenic nitrogen deposition in Rocky Mountain alpine tundra. *Ambio*, 514–517.

Brienen, R. J. W., Gloor, E., & Zuidema, P. A. (2012). Detecting evidence for CO 2 fertilization from tree ring studies: The potential role of sampling biases. *Global Biogeochemical Cycles*, *26*(1), n/a-n/a. https://doi.org/10.1029/2011GB004143

Chen, Y.-Y., Gardiner, B., Pasztor, F., Blennow, K., Ryder, J., Valade, A., … Luyssaert, S. (2018). Simulating damage for wind storms in the land surface model ORCHIDEE-CAN (revision 4262). *Geoscientific Model Development*, *11*(2), 771–791. https://doi.org/10.5194/gmd-11-771-2018

Chen, Y., Ryder, J., Bastrikov, V., McGrath, M. J., Naudts, K., Otto, J., … Luyssaert, S. (2016). Evaluating the performance of the land surface model ORCHIDEE-CAN on

water and energy flux estimation with a single- and a multi- layer energy budget scheme. *Geoscientific Model Development Discussions*, 1–35. https://doi.org/10.5194/gmd-2016-26

Cienciala, E., Altman, J., Doležal, J., Kopáček, J., Štěpánek, P., Ståhl, G., & Tumajer, J. (2018). Increased spruce tree growth in Central Europe since 1960s. *Science of The Total Environment*, *619–620*, 1637–1647. https://doi.org/https://doi.org/10.1016/j.scitotenv.2017.10.138

Deleuze, C., Pain, O., Dhôte, J.-F., & Hervé, J.-C. (2004). A flexible radial increment model for individual trees in pure even-aged stands. *Annals of Forest Science*, *61*(4), 327–335. https://doi.org/10.1051/forest:2004026

Ducoudré, N. I., Laval, K., & Perrier, A. (1993). SECHIBA, a New Set of Parameterizations of the Hydrologic Exchanges at the Land-Atmosphere Interface within the LMD Atmospheric General Circulation Model. *Journal of Climate*, *6*(2), 248–273. https://doi.org/10.1175/1520-0442(1993)006<0248:SANSOP>2.0.CO;2

Durka, W., Schulze, E.-D., Gebauer, G., & Voerkeliust, S. (1994). Effects of forest decline on uptake and leaching of deposited nitrate determined from 15N and 18O measurements. *Nature*, *372*(6508), 765–767. https://doi.org/10.1038/372765a0

Fatichi, S., Leuzinger, S., & Körner, C. (2014). Moving beyond photosynthesis: from carbon source to sink-driven vegetation modeling. *New Phytologist*, *201*(4), 1086–1095. https://doi.org/10.1111/nph.12614

Gaucherel, C., Guiot, J., & Misson, L. (2008). Changes of the potential distribution area of French Mediterranean forests under global warming. *Biogeosciences*, *5*(6), 1493–1504. https://doi.org/10.5194/bg-5-1493-2008

Groenendijk, P., van der Sleen, P., Vlam, M., Bunyavejchewin, S., Bongers, F., & Zuidema, P. A. (2015). No evidence for consistent long-term growth stimulation of 13 tropical tree

species: Results from tree-ring analysis. *Global Change Biology*. https://doi.org/10.1111/gcb.12955

Hale, S. E., Gardiner, B., Peace, A., Nicoll, B., Taylor, P., & Pizzirani, S. (2015). Comparison and validation of three versions of a forest wind risk model. *Environmental Modelling & Software*, *68*, 27–41. https://doi.org/10.1016/j.envsoft.2015.01.016

Haverd, V., Lovell, J. L., Cuntz, M., Jupp, D. L. B., Newnham, G. J., & Sea, W. (2012). The Canopy Semi-analytic Pgap And Radiative Transfer (CanSPART) model: Formulation and application. *Agricultural and Forest Meteorology*, *160*, 14–35. https://doi.org/10.1016/j.agrformet.2012.01.018

Hemery, G. E., Savill, P. S., & Pryor, S. N. (2005). Applications of the crown diameter–stem diameter relationship for different species of broadleaved trees. *Forest Ecology and Management*, *215*(1–3), 285–294. https://doi.org/10.1016/j.foreco.2005.05.016

Janssens, I. A., Dieleman, W., Luyssaert, S., Subke, J.-A., Reichstein, M., Ceulemans, R., … Law, B. E. (2010). Reduction of forest soil respiration in response to nitrogen deposition. *Nature Geoscience*, *3*(5), 315–322. https://doi.org/10.1038/ngeo844

Koutavas, A. (2008). Late 20th century growth acceleration in greek firs (Abies cephalonica) from Cephalonia Island, Greece: A CO2 fertilization effect? *Dendrochronologia*, *26*(1), 13–19. https://doi.org/10.1016/j.dendro.2007.06.001

Kramer, P. J., & Boyer, J. S. (1995). *Water relations of plants and soils.* San Diego, US: Academic Press, Book Marketing Department.

Krinner, G., Viovy, N., de Noblet-Ducoudré, N., Ogée, J., Polcher, J., Friedlingstein, P., … Prentice, I. C. (2005). A dynamic global vegetation model for studies of the coupled atmosphere-biosphere system. *Global Biogeochemical Cycles*, *19*(1). https://doi.org/10.1029/2003GB002199

Li, G., Harrison, S. P., Prentice, I. C., & Falster, D. (2014). Simulation of tree-ring widths

with a model for primary production, carbon allocation, and growth. *Biogeosciences*, *11*(23), 6711–6724. https://doi.org/10.5194/bg-11-6711-2014

Magnani, F, Mencuccini, M., & Grace, J. (2000). Age-related decline in stand productivity: the role of structural acclimation under hydraulic constraints. *Plant, Cell & Environment*, *23*(3), 251–263. https://doi.org/10.1046/j.1365-3040.2000.00537.x

Magnani, Federico, Mencuccini, M., Borghetti, M., Berbigier, P., Berninger, F., Delzon, S., … Grace, J. (2007). The human footprint in the carbon cycle of temperate and boreal forests. *Nature*, *447*(7146), 849–851. https://doi.org/10.1038/nature05847

McDowell, N., Pockman, W. T., Allen, C. D., Breshears, D. D., Cobb, N., Kolb, T., … Yepez, E. A. (2008). Mechanisms of plant survival and mortality during drought: why do some plants survive while others succumb to drought? *New Phytologist*, *178*(4), 719–739. https://doi.org/10.1111/j.1469-8137.2008.02436.x

Naudts, K., Ryder, J., McGrath, M. J., Otto, J., Chen, Y., Valade, A., … Luyssaert, S. (2015). A vertically discretised canopy description for ORCHIDEE (SVN r2290) and the modifications to the energy, water and carbon fluxes. *Geoscientific Model Development*, *8*(7), 2035–2065. https://doi.org/10.5194/gmd-8-2035-2015

Peper, P. J., McPherson, E. G., & Mori, S. M. (2001). Equations for predicting diameter, height, crown width, and leaf area of San Joaquin Valley street trees. *Journal of Arboriculture*, *27*(6), 306–317.

Pichler, V., Godinho-Ferreira, P., Zlatanov, T., Pichlerová, M., & Gregor, J. (2010). Changes in forest cover and its diversity. In *Forest Management and the Water Cycle* (pp. 209–224). Springer.

Poulter, B., MacBean, N., Hartley, A., Khlystova, I., Arino, O., Betts, R., … Peylin, P. (2015). Plant functional type classification for earth system models: results from the European Space Agency's Land Cover Climate Change Initiative. *Geoscientific Model*

Development, *8*(7), 2315–2328. https://doi.org/10.5194/gmd-8-2315-2015

Pretzsch, H. (2009). Forest dynamics, growth, and yield. In *Forest Dynamics, Growth and Yield* (pp. 1–39). Springer.

Rathgeber, C., Nicault, A., Guiot, J., Keller, T., Guibal, F., & Roche, P. (2000). Simulated responses of Pinus halepensis forest productivity to climatic change and CO2 increase using a statistical model. *Global and Planetary Change*, *26*(4), 405–421. https://doi.org/https://doi.org/10.1016/S0921-8181(00)00053-9

Reineke, L. H. (1933). Perfecting a stand-density index for even-aged forests, 627–638.

Rüger, N., Huth, A., Hubbell, S. P., & Condit, R. (2009). Response of recruitment to light availability across a tropical lowland rain forest community. *Journal of Ecology*, *97*(6), 1360–1368. https://doi.org/10.1111/j.1365-2745.2009.01552.x

Ryder, J., Polcher, J., Peylin, P., Ottlé, C., Chen, Y., van Gorsel, E., … Luyssaert, S. (2016). A multi-layer land surface energy budget model for implicit coupling with global atmospheric simulations. *Geoscientific Model Development*, *9*(1), 223–245. https://doi.org/10.5194/gmd-9-223-2016

SCHIMEL, D. S. (1995). Terrestrial ecosystems and the carbon cycle. *Global Change Biology*, *1*(1), 77–91. https://doi.org/10.1111/j.1365-2486.1995.tb00008.x

Seidl, R., Thom, D., Kautz, M., Martin-Benito, D., Peltoniemi, M., Vacchiano, G., … Reyer, C. P. O. (2017). Forest disturbances under climate change. *Nature Climate Change*, *7*(6), 395–402. https://doi.org/10.1038/nclimate3303

Sevanto, S., McDowell, N. G., Dickman, L. T., Pangle, R., & Pockman, W. T. (2014). How do trees die? A test of the hydraulic failure and carbon starvation hypotheses. *Plant, Cell & Environment*, *37*(1), 153–161. https://doi.org/10.1111/pce.12141

Shinozaki, K., Yoda, K., Hozumi, K., & Kira, T. (1964). A quantitative analysis of plant form-the pipe model theory: I. Basic analyses. *Japanese Journal of Ecology*, *14*(3), 97–

105. https://doi.org/10.18960/seitai.14.3_97

Sitch, S., Smith, B., Prentice, I. C., Arneth, A., Bondeau, A., Cramer, W., … Venevsky, S. (2003). Evaluation of ecosystem dynamics, plant geography and terrestrial carbon cycling in the LPJ dynamic global vegetation model. *Global Change Biology*, *9*(2), 161–185. https://doi.org/10.1046/j.1365-2486.2003.00569.x

Sperry, J. S., Nichols, K. L., Sullivan, J. E. M., & Eastlack, S. E. (1994). Xylem Embolism in Ring-Porous, Diffuse-Porous, and Coniferous Trees of Northern Utah and Interior Alaska. *Ecology*, *75*(6), 1736–1752. https://doi.org/10.2307/1939633

Su, H., Sang, W., Wang, Y., & Ma, K. (2007). Simulating Picea schrenkiana forest productivity under climatic changes and atmospheric CO2 increase in Tianshan Mountains, Xinjiang Autonomous Region, China. *Forest Ecology and Management*, *246*(2), 273–284. https://doi.org/https://doi.org/10.1016/j.foreco.2007.04.010

Viovy, N. (2016). CRUNCEP data set.

Vitousek, P. M., Aber, J. D., Howarth, R. W., Likens, G. E., Matson, P. A., Schindler, D. W., … Tilman, D. G. (1997). Human alteration of the global nitrogen cycle: sources and consequences. *Ecological Applications*, *7*(3), 737–750. https://doi.org/10.1890/1051-0761(1997)007[0737:HAOTGN]2.0.CO;2

Vuichard, N., Messina, P., Luyssaert, S., Guenet, B., Zaehle, S., Ghattas, J., … Peylin, P. (2019). Accounting for carbon and nitrogen interactions in the global terrestrial ecosystem model ORCHIDEE (trunk version, rev 4999): multi-scale evaluation of gross primary production. *Geoscientific Model Development*, *12*(11), 4751–4779. https://doi.org/10.5194/gmd-12-4751-2019

Yin, X., & Struik, P. C. (2009). C3 and C4 photosynthesis models: an overview from the perspective of crop modelling. *NJAS-Wageningen Journal of Life Sciences*, *57*(1), 27–38. https://doi.org/10.1016/j.njas.2009.07.001

Zaehle, S., & Friend, A. D. (2010). Carbon and nitrogen cycle dynamics in the O-CN land surface model: 1. Model description, site-scale evaluation, and sensitivity to parameter estimates. *Global Biogeochemical Cycles*, *24*(1). https://doi.org/doi:10.1029/2009GB003521

Zeide, B. (2010). Comparison of self-thinning models: an exercise in reasoning. *Trees*, *24*(6), 1117–1126. https://doi.org/10.1007/s00468-010-0484-z